Inorganic Chemistry

Article

pubs.acs.org/IC

Synthesis, Characterization, and Reactivity of Iron(III) Complexes Supported by a Trianionic ONO^{3-} Pincer Ligand

Matias E. Pascualini,[†,‡] Natali V. Di Russo,[†] Pedro A. Quintero,[§] Annaliese E. Thuijs,[†,‡] Dawid Pinkowicz,[∥,#] Khalil A. Abboud,[†,‡] Kim R. Dunbar,[∥] George Christou,[†,‡] Mark W. Meisel,[§] and Adam S. Veige*[,†,‡]

[†]Department of Chemistry, [‡]Center for Catalysis, and [§]Department of Physics and National High Magnetic Field Laboratory, University of Florida, Gainesville, Florida 32611, United States

[∥]Department of Chemistry, Texas A&M University, College Station, Texas 77842-3012, United States

[#]Faculty of Chemistry, Jagiellonian University, Ingardena 3, 30-060 Kraków, Poland

Supporting Information

ABSTRACT: Synthetic and characterization results of a new family of Fe(III) compounds stabilized by a trianionic $[CF_3{-}ONO]^{3-}$ pincer-type ligand are reported. The ligand possesses three negatively charged donors constrained to the meridional positions that provide sufficient electron density to stabilize high-valent metal complexes. Using the redox-insulated $[CF_3{-}ONO]^{3-}$, pentacoordinated square-pyramidal $\{[CF_3{-}ONO]\text{-}FeCl_2\}\{LiTHF_2\}_2$ (**3**), dimeric μ-DME$\{[CF_3{-}ONO]\text{-}FeDME\}_2$ (**4**), trigonal bipyramidal $[CF_3{-}ONO]Fe(bpy)$ (**5**), and octahedral $[CF_3{-}ONO]Fe(bpy)H_2O$ (**5·H$_2$O**) complexes are synthesized. An interesting feature of the $[CF_3{-}ONO]^{3-}$ pincer-type ligand is its ability to coordinate the metal center in both the more common meridional positions or occupying a face of a trigonal bipyramidal complex. The molecular structure of **3** contains structural features similar to those of a rare square-planar high-spin Fe(II) complex, and the important role of the counterions in stabilizing a square-plane is emphasized. SQUID magnetometry measurements of **3** reveal its high-spin character, and cyclic voltammetry measurements indicate high oxidation state species are unstable. However, all compounds can be reduced, and in particular **5** displays a reversible reduction event at −2255 mV versus ferrocene (Fc^+/Fc) that can be assigned to either the Fe^I/Fe^0 couple or 2,2′-bipyridine reduction.

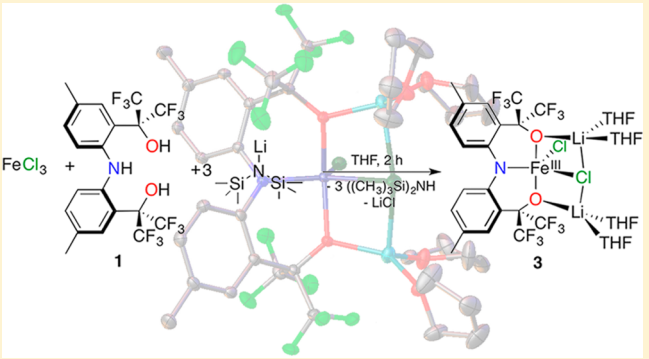

INTRODUCTION

Interest in pincer and pincer-type ligands arises from the possibility of fine-tuning the electronic and geometric properties of metal complexes through straightforward modification of the ancillary ligand. This versatile ligand class constrains three donor atoms to the meridional plane, resulting in coordinatively unsaturated metal complexes that are ideally suited for catalytic applications.[1−4] Trianionic pincer ligands originate as a subset of pincer ligands and are best suited to stabilize high-valent metal ions (M^{n+}, $n \geq 3$) by providing three negatively charged donors to satisfy the electronic needs of electron-deficient metal centers.[5] In the past decade, trianionic pincer ligands featuring NCN,[6−9] OCO,[10−21] NNN,[22−26] CCC,[27] SNS,[28] and ONO[25,29−38] arrangements of donor atoms were synthesized, and a recently published review article summarizes the latest achievements in this field.[5]

Trianionic pincer ligands provide a convenient framework for the development of new Fe(III) compounds. A catechol-based redox-active $[ONO^{cat}]H_3$ pincer ligand that can range from monoanionic to trianionic appeared in the literature for the first time in 1975[39] (Scheme 1), and since then several groups worked to expand its scope coordinating it to different metal centers.[25,35,36,38−43] Wieghardt and co-workers used it to synthesize a Cu(II) catalyst for aerobic oxidation of primary alcohols demonstrating for the first time the catalytic potential of complexes featuring this ligand.[43] The noninnocent trianionic $[ONO^{cat}]^{3-}$ catecholate ligand can act as a reservoir of electrons, being able to deliver one or two electrons to produce the radical dianionic $[ONO^{sq}]^{2-}$ semiquinonate or the monoanionic $[ONO^{q}]^{-}$ quinonate, respectively. The ligand's accessibility to multiple oxidation states allows first row transition metals, frequently constrained to one-electron redox chemistry, to perform multiple electron redox reactions usually involved in bond-making and bond-breaking processes.[34,36,44] Using the monoanionic quinonate form of the ligand, Heyduk and co-workers synthesized an Fe(III) complex capable of disulfide reductive elimination, where the ligand

Received: September 16, 2014
Published: November 24, 2014

   dx.doi.org/10.1021/ic502251p | Inorg. Chem. 2014, 53, 13078−13088

Scheme 1[a]

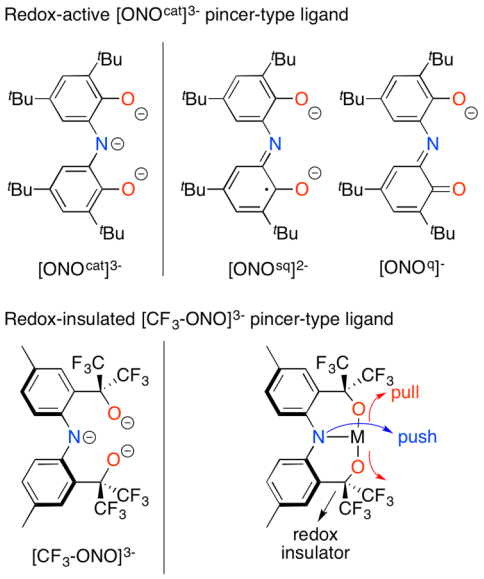

[a](top) Trianionic redox-active $[ONO^{cat}]^{3-}$ pincer-type ligand and its one- and two-electron oxidized forms. (bottom) Trianionic redox-insulated $[CF_3{-}ONO]^{3-}$ pincer ligand and its pull-push effect design.

accepts the two required electrons leaving the metal center's oxidation state unchanged.[34] In contrast, the recently reported 2,2′-(azanediylbis(3-methyl-6,1-phenylene))bis(1,1,1,3,3,3-hexafluoropropan-2-ol) $[CF_3{-}ONO]H_3$ (**1**) pincer-type ligand features heavily fluorinated alkoxide donors that act as redox insulators, preventing ligand noninnocence (Scheme 1).[31] The combination of these electron-withdrawing features with the central amido donor creates a push−pull electronic effect capable of enhancing the nucleophilicity of W−C multiple bonds.[31] Compared to the catechol-based ONO, the $[CF_3{-}ONO]^{3-}$ possesses one extra C in the flanking arms, allowing the formation of six-membered metalacycles, thus rendering the ligand more flexible. Finally, the four bulky CF_3 groups attached to the pendant arms are located in close proximity to the metal center providing it with additional steric protection that prevents coordination of two ONO ligands. The undesired coordinatively saturated $M[ONO]_2$ species represented a challenge in the development of complexes bearing the catechol-based ONO ligand.[40−42] Recently, our group demonstrated the applicability of **1** to iron chemistry and its success in stabilizing rare geometries and electronic structures by synthesizing a rare high-spin square-planar Fe(II) complex $\{[CF_3{-}ONO]FeCl_2\}\{Li(Sv)_2\}_2$ (**2**; Sv = tetrahydrofuran (THF), Et_2O).[33]

Herein, we present the synthesis of a family of Fe(III) compounds supported by the trianionic pincer ligand $[CF_3{-}ONO]^{3-}$. Characterization of the new complexes includes X-ray crystallography, superconducting quantum interference device (SQUID) magnetometry, electron paramagnetic resonance (EPR) spectroscopy, density functional theory (DFT) calculations, and cyclic voltammetry (CV) measurements.

RESULTS AND DISCUSSION

Molecular Structure of the Pincer-type Ligand $[CF_3{-}ONO]H_3$ (1). Synthesized according to published procedures, the $[CF_3{-}ONO]H_3$ (**1**) pincer-type ligand exhibits an interesting ^{19}F NMR spectrum.[31] Metalated $[CF_3{-}ONO]^{3-}$ typically exhibits well-resolved quartets;[30−32] however, as the free ligand in C_6D_6, the fluorine atoms resonate as two broad resonances indicating a fluxional process occurs in solution.[31] Insight into the origin of the fluxional behavior comes from the molecular structure as determined by single-crystal X-ray diffraction. Crystals deposit upon cooling a concentrated pentane solution of **1** to −35 °C. Figure 1 depicts the solid-state molecular structure of **1**, and Table 1 lists structural refinement data. Ligand **1** in the solid state is pseudo C_2-symmetric. Contributing to the low symmetry, the two tolyl rings twist (dihedral C4−C3−C13−C14 = 73.26(35)°) to reduce the steric interaction between *ortho*-hydrogen atoms. The sp^3-hybridized N1 forms a hydrogen-bonding interaction with H2 (d = 1.82(2) Å). Also, H1 forms a H-bond interaction with O2 (d = 2.038(19) Å), and H3 forms a hydrogen-bonding interaction with O1 in the adjacent molecule (d = 2.10(2) Å). These hydrogen-bonding interactions have an effect on the temperature-dependent ^{19}F NMR spectrum of **1**. Interestingly, the two fluorine resonances coalesce at 45 °C (E_a = 21.8(0.4) kcal mol^{-1}). Presumably, at 45 °C there is free rotation around the aryl−$C(CF_3)_2OH$ bond, while at 25 °C hydrogen bonding slows this rotation resulting in two sets of signals.

Synthesis and Molecular Structure of $\{[CF_3{-}ONO]FeCl_2\}\{LiTHF_2\}_2$ (3). Deprotonation of proligand **1** using 3 equiv of lithium hexamethyldisilazide ($LiN(SiMe_3)_2$) in THF, followed by subsequent addition to a THF solution of $FeCl_3$, results in an instantaneous color change from yellow to dark blue. Stirring the reaction for 2 h, removing all volatiles, and then adding toluene provides a green solution and insoluble LiCl. Filtration to remove LiCl and evaporation of the filtrate in vacuo provides analytically pure **3** in 73% yield according to Scheme 2. A ^1H NMR spectrum of **3** exhibits broadened paramagnetic spectral signatures not suitable for structural assignment. Complex **3** crystallizes from a concentrated THF/pentane solution at −35 °C as green rod-shaped crystals suitable for X-ray analysis.

Depicted in Figure 1 is the molecular structure of **3**. Table 1 lists structure refinement data, and Table 2 lists pertinent metric parameters. Interestingly, the Fe(III) center adopts a distorted square-pyramidal geometry within a C_1-symmetric environment imposed by the steric repulsion of the tolyl rings, which cannot lie coplanar. Atoms O1, N1, O2, and Cl2 form the basal plane, and Cl1 occupies the apical position. The Addison parameter (τ),[45] which is an index of distortion from square-pyramidal to trigonal-bipyramidal geometry, is 0.22. This value is significantly closer to an ideal square pyramid than the τ = 0.55 reported by Mindiola et al. for the PNP pincer complex $[(PNP)FeCl_2]$ (PNP = N[2-$P(CHMe_2)_2$-4-methylphenyl]$_2^-$).[46] The presence of the two Li counterions in **3** renders the Fe1−Cl2 (2.4252(15) Å) distance 0.1152(19) Å longer than the Fe1−Cl1 bond (2.3100(11) Å). The Li atoms are coplanar with the basal plane, and each distorted tetrahedral Li interacts with an oxygen atom from the pincer ligand, two THF molecules, and the same Cl atom (Cl2). In this respect, complex **3** bears a striking resemblance to the square planar complex **2** (see Figure 5 for a drawing).[33] In complex **2**, the square plane also comprises the pincer O, N, O, and a Cl atom that also interacts with two Li counterions bound to THF or Et_2O solvent molecules. DFT calculations of **2** show that the Li atoms play an important role in maintaining planarity, and removing them results in distortion to a tetrahedral geometry. In addition, for **2** the electrostatic attraction from the Li atoms, the strong trans influence of the amido N atom, and the σ-

dx.doi.org/10.1021/ic502251p | Inorg. Chem. 2014, 53, 13078−13088

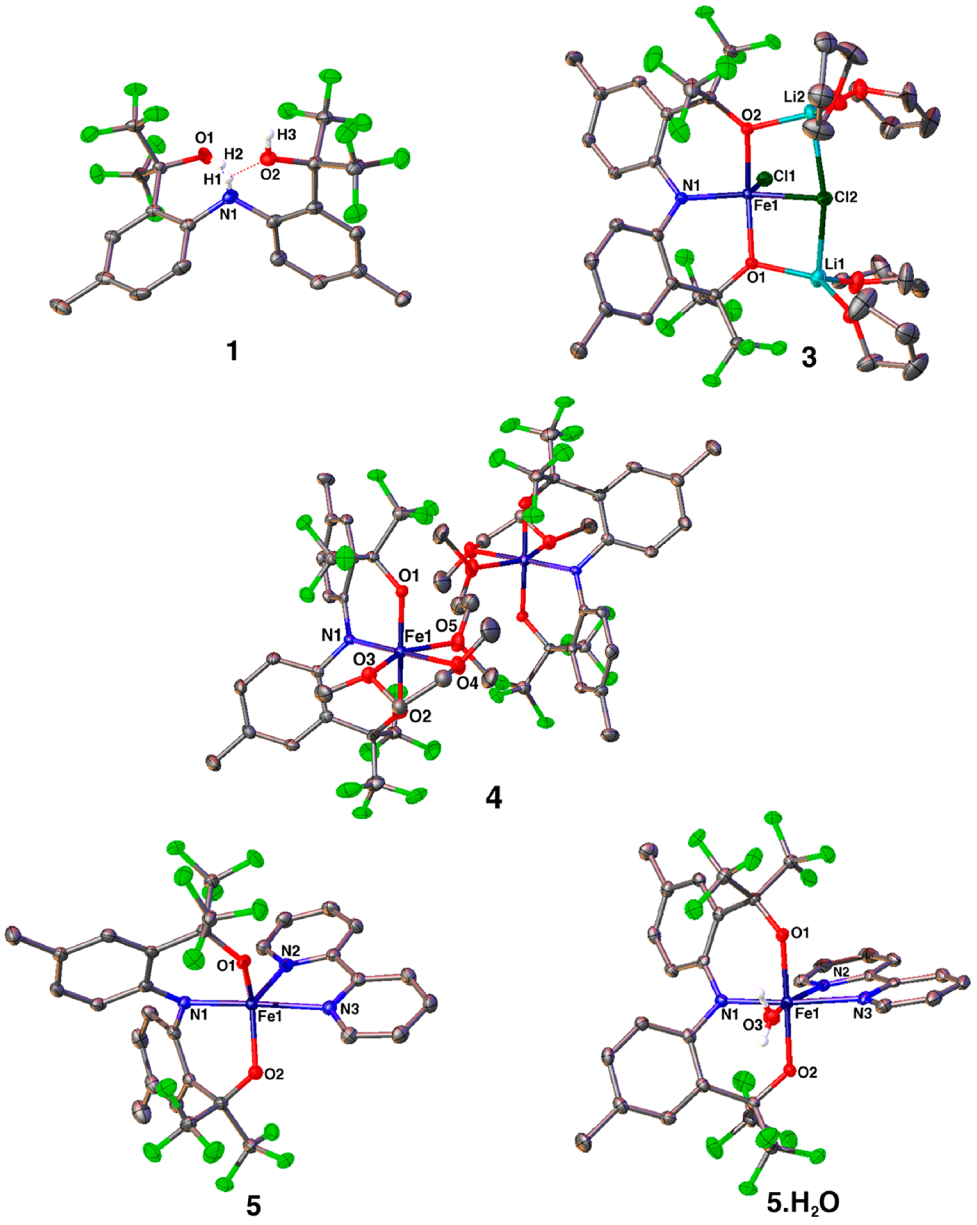

Figure 1. Molecular structures of **1**, **3**, **4**, **5**, and **5·H$_2$O**. Ellipsoids are drawn at 50% probability level. Hydrogen atoms were removed for clarity, except H1, H2, and H3 in **1** and H_2O hydrogens in **5·H$_2$O**.

donation of the alkoxides result in an overly elongated Fe−Cl bond (2.3888(9) and 2.338(3) Å for the two crystallographically unique molecules in the unit cell), which is critical to favoring the high-spin state.[33] In the case of **3**, the same factors result in the Fe1−Cl2 distance of 2.4252(15) Å being much longer than the one observed for [(PNP)FeCl$_2$] (2.2694(6) Å).[46] In addition, the sp^2-hybridized N1 atom adopts a trigonal planar geometry with the sum of the angles equal to 360.0(6)° and is capable of π-donating into the d-orbital manifold via its p-orbital resulting in a short Fe1−N1 bond distance of 1.926(4) Å. Other diaryl amido bond distances featuring significant π-donation have comparable lengths.[46]

Synthesis and Molecular Structure of μ-DME{[CF$_3$−ONO]FeDME}$_2$ (4). Attempts to remove the Cl ligands from complex **3** using AgPF$_6$ results in oxidation and decomposition. However, using 2 equiv of TlPF$_6$ to abstract the chloride ions in dimethoxyethane (DME) provides a green solution and copious white precipitate. Stirring for 20 min and removing the inorganic salts by filtration results in a green solution. Removing all volatiles under vacuum and washing the resulting green powder with pentane provides dinuclear complex **4** in 37% yield (Scheme 2). The ^{1}H NMR spectrum of **4** exhibits four broad resonances not suitable for structural assignment (see Supporting Information). However, X-ray quality single crystals grow upon cooling a concentrated DME/pentane solution of **4** to −35 °C.

Figure 1 depicts the molecular structure of **4**, Table 1 lists refinement data, and Table 2 lists important bond angles and lengths. The asymmetric unit consists of two half-dimers (each located on an inversion center). The dimers contain two Fe(III) ions in a distorted octahedral coordination geometry with a DME molecule linking them. Both dimers are chemically equivalent but crystallographically independent. All the bond distances between the independent dimers vary by 0.0125(25) Å or less; for example, the Fe1−O1 and Fe1−O2 average bond

dx.doi.org/10.1021/ic502251p | *Inorg. Chem.* 2014, 53, 13078−13088

Table 1. Selected Crystallographic Data for Compounds 1, 3, 4, 5, and 5·H_2O

	1	3	4	5	5·H_2O
empirical formula	$C_{22.50}H_{18}F_{12}NO_2$	$C_{36}H_{44}Cl_2F_{12}FeLi_2NO_6$	$C_{52}H_{54}F_{24}Fe_2N_2O_{10}$	$C_{30}H_{20}F_{12}FeN_3O_2$	$C_{38}H_{42}F_{12}FeN_3O_7$
molar mass (g/mol)	562.38	955.35	717.34	738.34	936.59
T (K)	100(2)	100(2)	100(2)	100(2)	100(2)
crystal system	monoclinic	monoclinic	triclinic	monoclinic	triclinic
space group	$P2_1/n$	$C2/c$	$P\bar{1}$	$P2_1/n$	$P\bar{1}$
a (Å)	11.3214(5)	31.479(2)	12.2812(8)	13.5244(6)	11.3312(3)
b (Å)	18.4917(8)	12.6762(10)	13.3854(9)	15.9041(7)	11.9100(3)
c (Å)	11.9749(5)	27.582(2)	18.4188(13)	14.1139(6)	17.0755(5)
α (deg)	90	90	77.720(2)	90	104.924(2)
β (deg)	111.883(1)	117.561(4)	86.605(2)	97.184(2)	102.833(2)
γ (deg)	90	90	77.097(2)	90	103.035(2)
V (Å^3)	2326.33(17)	9757.1(13)	2883.6(3)	3012.0(2)	2070.99(10)
Z	4	8	2	4	2
ρ_{calcd} (g/cm^3)	1.606	1.301	1.652	1.628	1.502
μ (mm^{-1})	0.167	0.502	0.639	0.609	0.469
F(000)	1136	3912	1456	1484	962
crystal size (mm)	0.37 × 0.11 × 0.11	0.30 × 0.06 × 0.05	0.10 × 0.05 × 0.03	0.23 × 0.21 × 0.10	0.40 × 0.23 × 0.18
θ range (deg)	2.11−27.50	1.63−27.50	1.59−26.74	1.94−27.50	1.86−27.50
reflns collected	31 270	77 038	48 530	49 897	48 219
independent reflns	5291	11 200	12 245	6926	9511
R_{int}	0.0187	0.1505	0.0690	0.0463	0.0602
GOF on F^2	0.941	0.856	0.821	1.071	0.955
R_1, R_2 [$I > 2\sigma(I)$]	0.0348, 0.0877	0.0679, 0.1750	0.0372, 0.0626	0.0291, 0.0774	0.0380, 0.0879
R_1, R_2 (all data)	0.0426, 0.0930	0.1454, 0.1975	0.0858, 0.0705	0.0391, 0.0813	0.0556, 0.0942

Scheme 2. Synthesis of Fe(III) Complexes Supported by a Trianionic Pincer-type Ligand

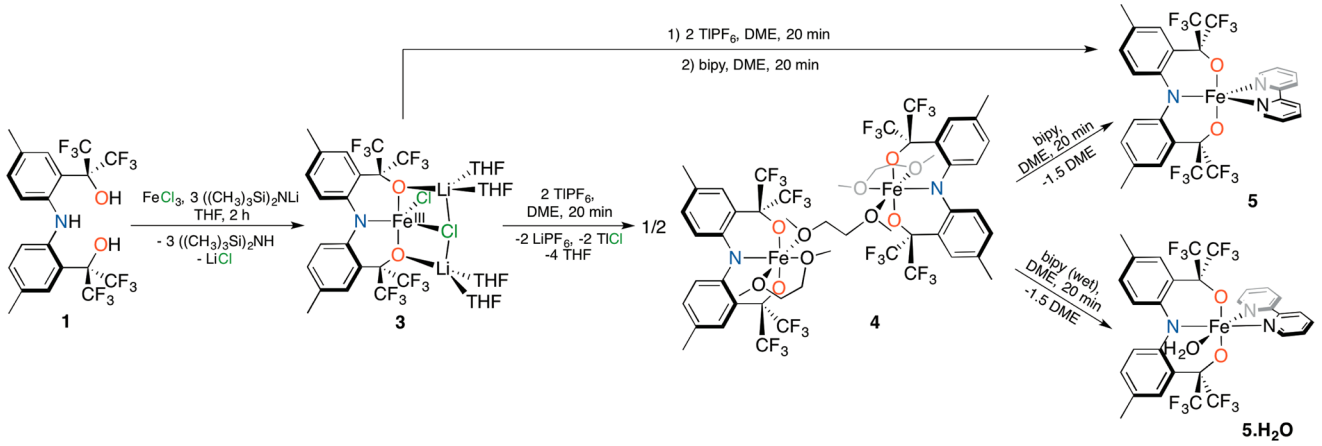

Table 2. Selected Bond Distances (Å) and Angles (deg) for Compounds 3, 4, 5, and 5·H_2O

	3	4[a]	5	5·H_2O
Fe1−N1	1.926(4)	1.9480(28)	1.9190(12)	1.9491(15)
Fe1−N2			2.1324(13)	2.1746(15)
Fe1−N3			2.1564(12)	2.1930(15)
Fe1−O1	1.980(3)	1.8879(24)	1.8689(10)	1.9174(13)
Fe1−O2	1.973(3)	1.8914(24)	1.8964(11)	1.9230(13)
Fe1−O3		2.2176(25)		2.1350(15)
Fe1−O4		2.2373(25)		
Fe1−O5		2.1708(25)		
Fe1−Cl1	2.3100(11)			
Fe1−Cl2	2.4252(15)			
O1−Fe1−O2	155.72(14)	177.03(11)	128.62(5)	176.47(5)
N2−Fe1−N3			75.30(5)	74.50(6)

[a]Average value for the crystallographically independent dimers.

dx.doi.org/10.1021/ic502251p | Inorg. Chem. 2014, 53, 13078−13088

lengths are 1.8870(24) Å and 1.8914(24) Å, respectively. Compared to complex **3**, the Fe−O_{pincer} bond lengths are considerably shorter by 0.0869(27) Å. This difference is understandable considering the strongly π-donating Cl^- ligands in **3** are lost and the alkoxides of the pincer compensate for the reduced electron density by increasing their π-donation. The Fe1−$N1_{avg}$ bond (1.9480(28) Å) exerts a strong *trans* influence on O4 to give a long Fe1−$O4_{avg}$ bond distance of 2.2373(25) Å in comparison with the mutually *trans* Fe1−$O3_{avg}$ (2.2176(25) Å) and Fe1−$O5_{avg}$ (2.1708(25) Å) bonds. Reflecting less distortion than in **3** (∠O1−Fe1−O2 = 155.72(14)°), complex **4** contains a nearly linear bond angle of 177.03(11)° for O1−Fe1−$O2_{avg}$.

Synthesis and Molecular Structure of [CF_3−ONO]Fe(bpy) (5) and of [CF_3−ONO]Fe(bpy)H_2O (5·H_2O). Treating **4** with 0.5 equiv of 2,2′-bipyridine in DME results in a subtle color change from green to bluish green. Stirring the reaction mixture for 20 min and removing all volatiles under vacuum generates a blue-green residue. Washing this residue with pentane produces an analytically pure microcrystalline powder of **5** in 50% yield (Scheme 2). A ^{1}H NMR spectrum of **5** exhibits broadened paramagnetic spectral signatures not suitable for structural assignment. If the 2,2′-bipyridine is not recrystallized and intensively dried, exposing it to the same reaction conditions results in the aquo complex **5·H_2O** (Scheme 2). Subjecting **5·H_2O** to prolonged drying times under reduced pressure does not result in formation of **5**. A ^{1}H NMR spectrum of **5·H_2O** contains the same number of signals as **5** (presumably the H_2O protons in **5·H_2O** are too broad to be observed). Also, the chemical shifts of the broadened paramagnetic resonances are only slightly shifted from those of **5**. An alternative synthetic route to **5** from **3** consists of in situ generation of **4** by addition of $TlPF_6$ and subsequent addition of 2,2′-bipyridine to produce **5** in 72% yield (Scheme 2). Cooling a saturated DME/pentane solution of **5** or **5·H_2O** to −35 °C produces single crystals suitable for X-ray interrogation.

Figure 1 depicts the molecular structures of **5** and **5·H_2O**, Table 1 lists refinement data, and Table 2 lists pertinent metric parameters. Complex **5·H_2O** comprises a distorted octahedral Fe(III) ion coordinated by the $[CF_3−ONO]^{3-}$ pincer-type ligand, a bidentate 2,2′-bipyridine, and a H_2O molecule. The main distortion from an ideal octahedral geometry is the acute angle (74.50(6)°) imposed by the 2,2′-bipyridine N atoms, since the O1−Fe1−O2 bite angle is nearly linear (176.47(5)°). The strong *trans* influence of the pincer amido N atom renders the Fe1−N3 distance 0.2439(21) Å longer than the Fe1−N1 distance (1.9491(15) Å). The homoleptic Fe(III) compound $[Fe(bpy)_3]^{3+}$ possesses Fe−N_{bpy} average bond lengths of 1.961(7) Å;[47] 0.223(7) Å shorter than the average Fe1−N_{bpy} bond in **5·H_2O**, highlighting that the trianionic $[CF_3−ONO]^{3-}$ pincer-type ligand is more capable of satisfying the Fe atom's acidity. Without a sixth ligand, **5** adopts a distorted trigonal bipyramidal geometry (τ = 0.82).[45] The pincer N atom occupies one axial position, and N3 of the bpy occupies the opposite position. The O1−Fe1−O2 pincer bite angle (128.62(5)°) is significantly smaller than in **3** (155.72(14)°), **4** (177.03(11)°), and **5·H_2O** (176.47(5)°), reflecting its occupation of equatorial positions. Similar to **5**, complexes [^{t}BuOCO]Cr^V(O)(THF)[14] (126.89(8)°) and {[^{t}BuOCO]-Cr^{IV}(THF)}$_2$(μ-O)[15] (125.50(7)°) also exhibit small bite angles and feature a pincer ligand spanning the equatorial sites of a trigonal bipyramid instead of the most commonly observed orientation of meridional coordination within a square pyramid or octahedral complex.

Redox Behavior of Compounds 3−5. The electrochemical properties of complexes **3**−**5** were investigated in acetonitrile/0.1 M Bu_4NPF_6 using a 3 mm glassy carbon electrode. Figure 2 depicts the resulting cyclic voltammograms.

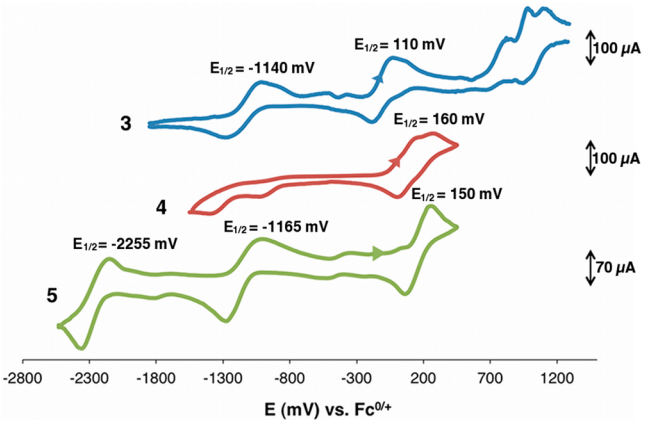

Figure 2. Cyclic voltammograms of complexes **3**−**5** in acetonitrile using 0.1 M Bu_4NPF_6 as supporting electrolyte and scan rates of 100, 200, and 50 mV/s, respectively. Working electrode: 3 mm glassy carbon. Reference electrode: Ag/AgCl. Auxiliary electrode: Pt wire.

All values in this work are reported vs ferrocene (Fc/Fc^+). To assess the reversibility of these redox processes the dependence of the potential with the scan rate, and the stability of the cathodic and anodic waves upon repeated scanning (see Supporting Information for more details), were tested. All compounds present two common features: a quasi-reversible response with $E_{1/2} \approx 150$ mV (Fe^{III}/Fe^{II}) and a second redox process, quasi-reversible for **3** and **5**, and irreversible for **4**, with $E_{1/2} \approx -1150$ mV (Fe^{II}/Fe^{I}). In the case of **4**, a shoulder appears in the cathodic wave at 140 mV, attributable to cooperativity between the two iron centers, or to the substitution of a labile DME ligand with an acetonitrile solvent molecule, resulting in different molecules with slightly different reduction potentials.[48] In addition, all complexes present irreversible oxidation events beginning near 700 mV. Attempts to chemically oxidize complexes **3**−**5** with iodosobenzene lead to intractable mixtures. Moreover, complex **5** presents a quasi-reversible response with $E_{1/2} = -2255$ mV, tentatively assigned to the Fe^I/Fe^0 couple[49] or a ligand-centered reduction of 2,2′-bypiridine.[50]

The potentials obtained from the CV experiments highlight the inductive effect of the fluorinated alkoxide arms of the pincer ligand on its σ-donating capability. In principle, the trianionic charge of the ligand should stabilize high oxidation states, as in the case of corroles, which are able to stabilize Fe(IV) species.[51,52] However, the $[CF_3−ONO]^{3-}$ ligand is a weaker σ-donor, and as a consequence the $E_{1/2}$ value for the Fe^{III}/Fe^{II} couple in **2** is higher than that for the Fe^{IV}/Fe^{III} couple in [Fe(cor)Cl] ($E_{1/2}$ = 44 mV),[51] and the $E_{1/2}$ value for the Fe^{II}/Fe^{I} couple in **5** is higher than that of Fe^{IV}/Fe^{III} couple in pyridine-bound iron corroles ($E_{1/2} = -1436$ mV).[52] In agreement with these observations, all attempts to oxidize Fe(III) compounds **3**−**5** were unsuccessful. Furthermore, while some iron corroles[51,52] decompose upon reduction from Fe(III), the poor σ-donation capability of the fluorinated alkoxides allows reduction to Fe(I) in the cases of the

dx.doi.org/10.1021/ic502251p | Inorg. Chem. 2014, 53, 13078−13088

mononuclear complexes **2** and **5**, and possibly to Fe(0) in the case of **5**. Interestingly, the potentials of the Fe^{II}/Fe^{I} and Fe^{I}/Fe^{0} couples are well within the range of those reported for iron porphyrins.[49]

EPR Spectroscopy and Magnetic Susceptibility Measurements of Compound 3. The X-band EPR spectrum of **3** collected as a frozen toluene solution at 10 K (Figure 3) exhibits features at g_{eff} = 2.37, 3.15, 5.54, and 9.42. Using EasySpin,[53] the spectrum can be simulated considering an S = 5/2 system with g values of g_x = 1.96, g_y = 2.02, g_z = 1.90. The complex exhibits appreciable zero-field splitting, with a D value of 3.1 cm^{-1}, and an intermediate degree of rhombicity, with an E value of −0.13 D. Halogen-bound Fe(III) S = 5/2 porphyrin complexes display similar D values.[54] The position of the features is similar to those reported for a series of Fe(III) S = 5/2 complexes supported by a trianionic pyrrolide-armed tripodal ligand.[55] The feature with g_{eff} = 2.37 overlaps with the wider feature at g_{eff} = 3.15. These features are transitions of components of the m_s = ± 1/2 and m_s = ± 1/2, ± 3/2 states, respectively. The feature with g_{eff} = 5.54 corresponds to m_s = ± 3/2 state transitions, and finally the feature with g_{eff} = 9.42 originates from m_s = ± 5/2 state transitions.[56]

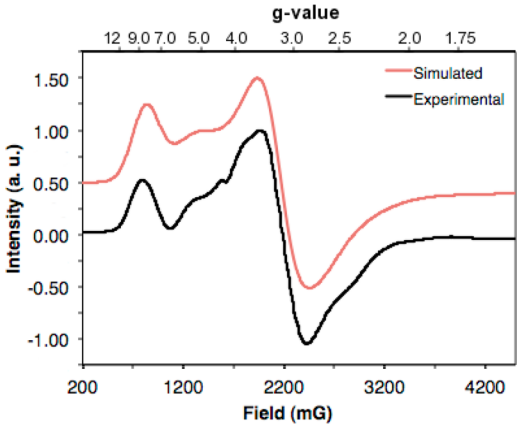

Figure 3. X-band EPR spectra of **3** collected as a frozen toluene solution at 10 K, simulated using EasySpin[53] with values of g_x = 1.96, g_y = 2.02, g_z = 1.90, D = 3.1 cm^{-1}, and E = −0.13 D.

Magnetic susceptibility measurements of **3** in the 2−300 K temperature range using a 100 G field (Figure 4) reveal a room-temperature $\chi_M T$ value of 4.05 cm^3 K mol^{-1} (μ_{eff} = 5.69 μ_B). This value is consistent with the one expected for an S = 5/2 state (4.38 cm^3 K mol^{-1}, 5.92 μ_B) and with the solution value of 4.53 cm^3 K mol^{-1} (μ_{eff} = 6.02 μ_B), as determined by Evans method.[57] The $\chi_M T$ value steadily decreases with decreasing temperature, reaching 2.27 cm^3 K mol^{-1} (μ_{eff} = 4.26 μ_B) at 2 K. The D and E values derived from the EPR measurements also provide a good fit to the magnetic susceptibility data.

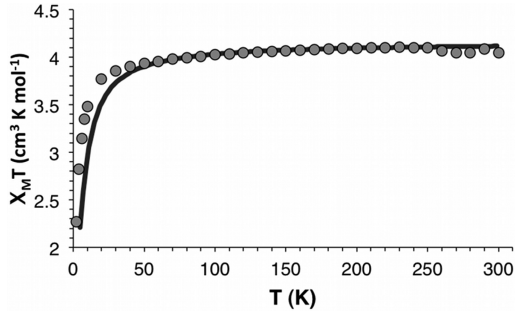

Figure 4. Temperature dependence of $\chi_M T$ for **3** measured using an applied field of 100 G. The line depicts the results obtained from an EasySpin[59] simulation[58] using S = 5/2, D = 3.1 cm^{-1}, E = −0.13 D, and g_x = 1.96, g_y = 2.02, g_z = 1.90.

Motivation for collecting alternating current (AC) magnetic susceptibility data of **3** comes from the work of Mindiola et al., who report a structurally similar Fe(III) PNP^{-1} pincer complex, [(PNP)$FeCl_2$], that is a mononuclear single molecule magnet.[46] AC magnetic susceptibility measurements of **3** were performed in the 1.8−300 K range using a 3.5 G AC field oscillating at frequencies up to 1000 Hz to probe both the spin state of the Fe(III) in the absence of an applied direct current (DC) field and to determine if the molecule exhibits slow magnetization relaxation. The AC in-phase $\chi'_M T$ is 4.05 cm^3 K mol^{-1} (μ_{eff} = 5.69 μ_B) at 300 K and remains essentially constant with decreasing temperature until ∼50 K, when it begins gradually decreasing until it reaches 2.30 cm^3 K mol^{-1} (μ_{eff} = 4.29 μ_B) at 1.8 K (see Supporting Information). Although noisier than the DC data, the AC data also support a spin of S = 5/2 for **3**. The AC out-of-phase χ''_M versus T plot is featureless (see Supporting Information), confirming that **3** does not exhibit slow magnetization relaxation despite its relatively large |D| value, and this result is consistent with a positive D-value as found by EPR measurements.

DFT Calculations of Compounds 3 and 5. The electronic structures of complexes **3** and **5** were examined using DFT at the B3LYP level of theory.[59,60] Compound **3** was modeled as **3′**, where the solvent molecules and counterions were removed for simplicity. When compared to the experimentally determined structures, the optimized geometries have bond lengths that differ by less than 0.1 Å. However, the τ parameters of the models do differ from their solid-state structures and are worth noting. The DFT-optimized complex **5′** has a subtle geometry change toward a square pyramidal structure evidenced by a decrease in τ from 0.82 (**5**) to 0.60 (**5′**). In the case of **3′**, the geometry change is much larger, since the calculated structure is best described as trigonal bipyramidal (τ = 0.74), while the molecular structure of **3** is closer to a square pyramid with τ = 0.22 (Figure 5, bottom).

The large geometry change of **3′** can be attributed to the absence of counterions. Because of their electrostatic attraction, the Li^+ ions play a key role in favoring structures with a square base. In complex **3**, the Li^+ ions are coplanar with the Fe and ligand donors forming the base of the square pyramid. The geometry relaxes toward a trigonal bipyramid, when the Li^+ ions are removed in **3′**. Attempts to synthesize the Na^+ analogue or to exchange the Li^+ ions with the bulkier Bu_4N^+ cations, to experimentally probe the counterion effect on the geometry, were unsuccessful.

The high-spin square-planar complex **2** displays a very similar arrangement of atoms in its square plane (Figure 5, top). Upon removal of the Li^+ ions and coordinated solvent, the geometry of **2** also distorts significantly toward the more common tetrahedral structure **2′** (Figure 5, top).[33] The electrostatic potential maps calculated for the X-ray and optimized conformations in the absence of Li^+ ions and solvent molecules provide further insight into the factors that trigger these conformational changes. These maps illustrate the charge distributions of the molecules, using a color spectrum where red represents the more negative electrostatic potential values. In the X-ray conformations, the more negative values are

dx.doi.org/10.1021/ic502251p | Inorg. Chem. 2014, 53, 13078−13088

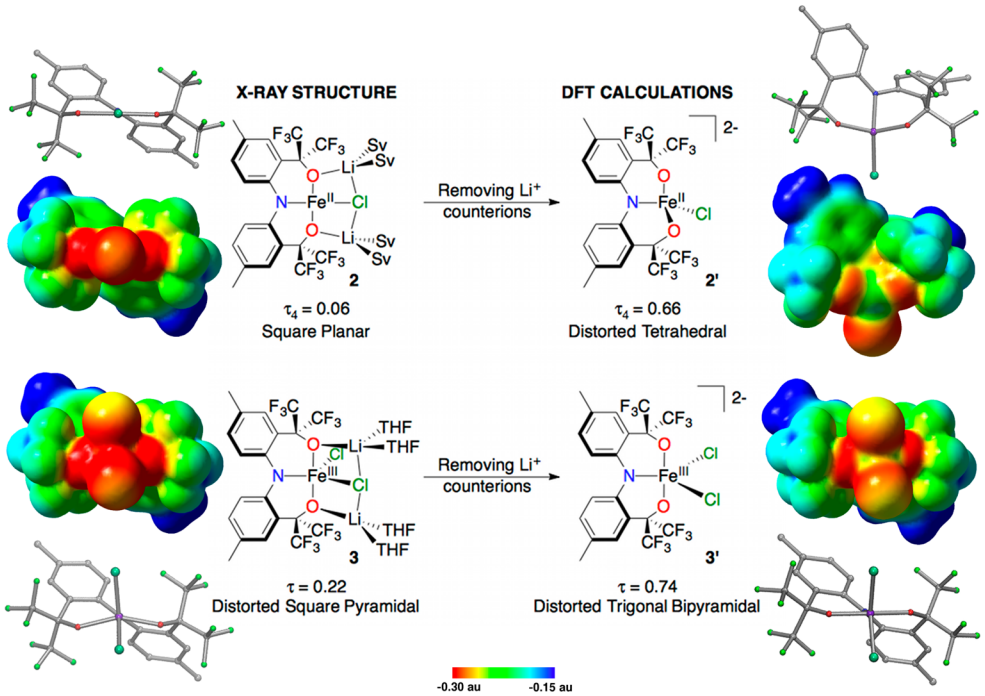

Figure 5. Geometry changes upon removal of Li^+ counterions for compounds **2** (top) and **3** (bottom). The electrostatic potential surface maps for the X-ray and optimized conformations are shown using a color spectrum where red represents the more negative electrostatic potential values (isovalue = 0.004). The same color scale was used in all cases.

located on the O and Cl atoms in the plane, so that placing the Li ions between an O and the Cl results in optimal electrostatic stabilization. In contrast, in the calculated structures the electrostatic potential on these atoms is less negative; thus, in the absence of the Li ions, distortion to trigonal bipyramidal prevails for **3′**. In the case of **2′**, the more favorable position for the Li^+ ions is on the same face of the molecule, but optimal charge compensation is limited by the electrostatic repulsion that takes place if the Li^+ ions are placed too close to each other. In **3′**, the optimum position would be close to the O atoms, where there would be some repulsion between the Li^+ ions because a Cl atom is not between them. In summary, in the X-ray conformation the larger degree of polarization results in a more favorable electrostatic interaction with the counterions, and positioning them in a square plane with a Cl atom between them minimizes their repulsion. These factors drive the conformations from the sterically preferred tetrahedral and trigonal bipyramidal geometries to the observed square planar and square pyramidal ones.

Applied successfully to analyze the molecular orbitals of other high-spin Fe compounds,[61,62] the orbitals resulting from spin-unrestricted calculations of **3′** and **5′** were analyzed using the bi-orthogonal corresponding orbital approach. For both **3′** (Figure 6) and **5′** (Figure 7), the singly occupied molecular orbitals (SOMOs) are principally Fe based with some π-antibonding contributions from the pincer O atoms. Accordingly, the spin density plots show that the unpaired electron density is mostly localized on the metal, with some contribution from the ligand donors. The most significant difference between **3′** and **5′** is the larger degree of delocalization of the electronic and spin densities in the case of **5′**, as reflected by the contribution of the pincer's tolyl ring to the third SOMO and the spin density plot. These results offer an explanation for the stability of the possible reduction of Fe(III) in **5** to Fe(0) that was observed by CV.

CONCLUDING REMARKS

This paper reports the successful synthesis of a new family of Fe(III) complexes supported by a trianionic $[CF_3{-}ONO]^{3-}$ pincer-type ligand. Synthesized from a readily available Fe salt, the basal plane of **3** bears a striking resemblance to the high-spin square-planar Fe(II) complex **2**. Both molecular structures feature a square-plane base consisting of the ONO ligand and a Cl atom. Two Li^+ counterions lie coplanar to the square planes, and each ion interacts with a pincer O and the Cl atom. DFT calculations reveal significant distortions toward a tetrahedron and a trigonal bipyramid for **2** and **3**, respectively, upon removal of the Li^+ ions. This result highlights the counterions' significant influence in dictating the geometry of molecular compounds, in this case by playing a key role in stabilizing a square base.

The redox-insulated $[CF_3{-}ONO]^{3-}$ presents a valuable alternative to the previously reported redox-active catechol-based ONO ligand for the synthesis of Fe complexes. The bulky CF_3 groups featured in the pincer's flanking arms provide enough steric protection to allow coordination of only one ONO ligand per metal, thus avoiding the coordinatively saturated $M[ONO]_2$ species that proved to be troublesome in the synthesis of complexes featuring the less sterically encumbered catechol-based ONO.[40−42] In addition, the $[CF_3{-}ONO]^{3-}$ pincer-type ligand bears one extra C in its flanking arms, allowing it to form six-membered metalacycles, which provide more flexibility to the ligand. This enhanced flexibility allows the ligand to coordinate in both a meridional and a facial fashion: although the $[CF_3{-}ONO]^{3-}$ has a preference for meridional positions, in complex **5** it occupies a face of the trigonal bipyramid.

SQUID magnetometry and EPR spectroscopy data of complex **3** are consistent with an $S = 5/2$ Fe(III) center and can be simulated using zero-field splitting parameters $D = 3.1$

dx.doi.org/10.1021/ic502251p | Inorg. Chem. 2014, 53, 13078−13088

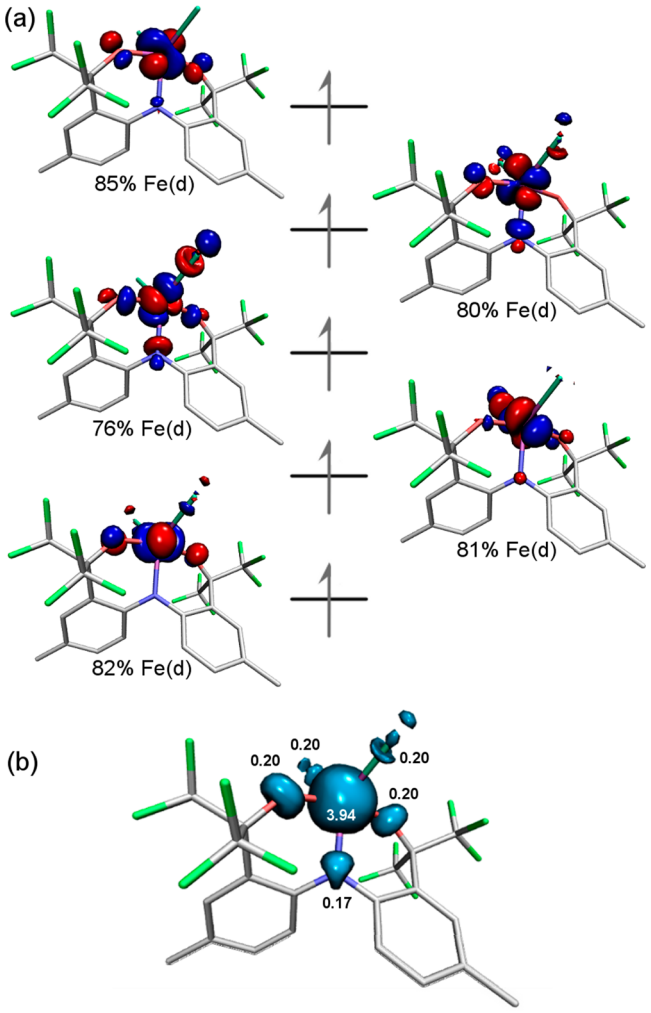

Figure 6. (a) Bi-orthogonalized molecular orbitals for **3**′ from a spin-unrestricted B3LYP DFT calculation; isovalue: 0.05. (b) Spin density plot obtained from a Mulliken population analysis; isovalue: 0.01 [cyan, positive spin density; gold, negative spin density (not observed)].

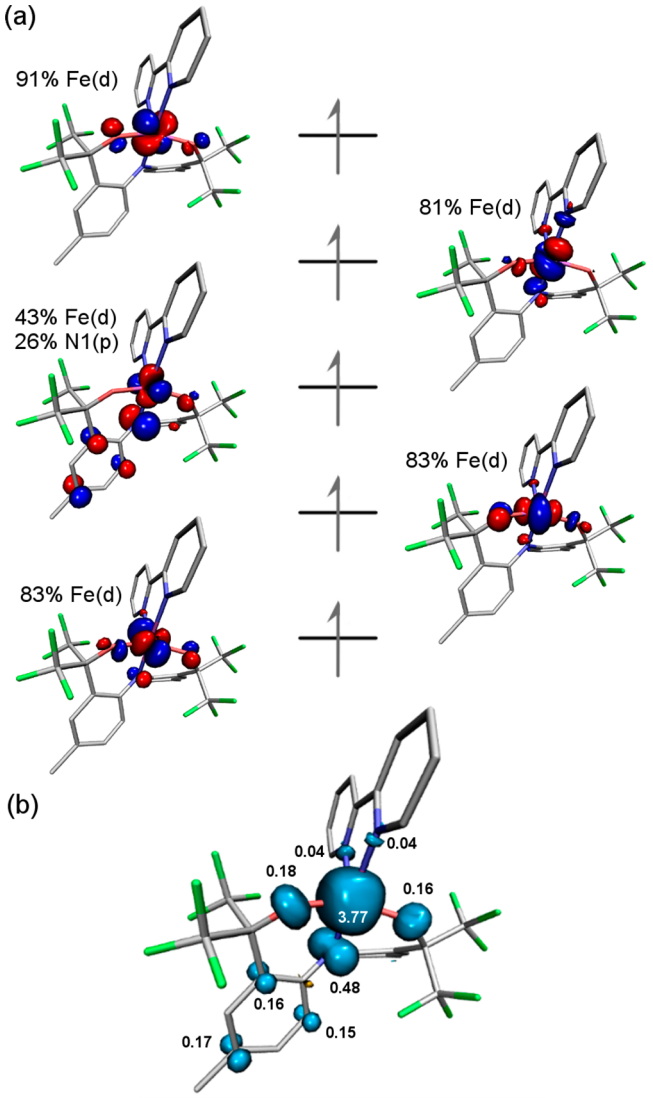

Figure 7. (a) Bi-orthogonalized molecular orbitals for **5**′ from a spin-unrestricted B3LYP DFT calculation; isovalue: 0.05. (b) Spin density plot obtained from a Mulliken population analysis; isovalue: 0.01 (cyan, positive spin density; gold, negative spin density).

cm^{-1} and $E = -0.13$ D. Halogen-bound Fe(III) $S = 5/2$ porphyrin complexes display similar D values.[54] CV measurements on **3**−**5** reveal that higher oxidation states are not stable. This behavior is strikingly different than that for Fe corroles, which can usually be oxidized to Fe(IV). The rigid macrocyclic structure of trianionic corroles brings the N donors in close proximity to the metal, enabling the stabilization of high oxidation states. In contrast, because of the flexible structure and the presence of heavily fluorinated alkoxides, the $[CF_3-ONO]^{3-}$ ligand is unable to stabilize Fe(IV) species. However, these properties result in effective stabilization of reduced Fe species, revealed by reversible reduction events corresponding to the Fe^{III}/Fe^{II} (**3**−**5**) and Fe^{II}/Fe^{I} (**3** and **5**) couples. In addition, complex **5** displays a reversible reduction event at −2255 mV versus Fc^+/Fc that can be assigned to the Fe^{I}/Fe^{0} couple or to 2,2′-bipyridine reduction. Future work in our lab will focus on the isolation of low-valent Fe species, since these have been used as catalysts for reactions such as cross-coupling[63] and hydrogenation.[64]

EXPERIMENTAL SECTION

General Conditions. Unless specified otherwise, all manipulations were performed under an inert atmosphere using standard Schlenk or glovebox techniques. Glassware was oven-dried before use. Pentane, toluene, tetrahydrofuran (THF), and 1,2-dimethoxyethane (DME) were dried using a GlassContours drying column. Deuterated benzene (benzene-d_6) (Cambridge Isotopes) was dried over sodium-benzophenone ketyl and distilled or vacuum-transferred and stored over 4 Å molecular sieves. $FeCl_3$ 98% (anhydrous) was purchased from Acros Organics and was used as received. NMR spectra were obtained on Varian Mercury Broad Band 300 MHz or Varian Mercury 300 MHz spectrometers. Chemical shifts are reported in δ (ppm). For ^1H NMR spectra the solvent resonance was referenced as an internal reference, and the baseline was corrected manually. EPR measurements were conducted using a Bruker Elexsys-500 spectrometer at the X-band microwave frequency at ∼9.6 Ghz at 10 K. The microwave frequency was measured with a built-in digital counter, and the magnetic field was calibrated using 2,2-diphenyl-1-picrylhydrazyl (DPPH; $g = 2.0037$). The temperature was controlled using an Oxford Instruments cryostat accurate within ±0.1 K. Modulation amplitude and microwave power were optimized for high signal-to-noise ratio and narrow peaks. CV was performed under a nitrogen

dx.doi.org/10.1021/ic502251p | Inorg. Chem. 2014, 53, 13078−13088

atmosphere using a standard three-electrode setup. A glassy carbon electrode (3 mm diameter) was used as a working electrode, a platinum wire was used as counter electrode, and Ag/AgCl was used as reference electrode. The measurements were made in 0.1 M Bu_4NPF_6 acetonitrile solution, and a 10 mM ferrocene solution was used as external reference. Bu_4NPF_6 99.0% was purchased from Sigma-Aldrich and was used as received. Electrodes were purchased from either BASi, Inc. or CH Instruments, Inc. Potential sweeps were controlled by a Princeton Applied Research Versastat II potentiostat. Variable-temperature DC and AC magnetic susceptibility data were collected in the 2.0−300.0 K range using a Quantum Design MPMS-XL SQUID magnetometer equipped with a 7 T DC magnet in an applied field of 100 G. The microcrystalline samples were restrained in eicosane to prevent torquing. Diamagnetic corrections using Pascal's constants were applied to the observed susceptibilities to obtain the molar paramagnetic susceptibility (χ_M). Elemental analyses were performed at Complete Analysis Laboratory Inc., Parsippany, New Jersey.

Density Functional Theory Calculations. Spin-unrestricted DFT calculations were carried out at the B3LYP[59,60] level of theory using Gaussian 09.[65] The LANL2DZ[66] basis set and an effective core potential were used for the Fe atoms, and 6-31G** was used for all other atoms. Initial geometries were derived from the corresponding crystal structures (after removing solvent molecules and counterions) and were subjected to optimization. Normal-mode analysis was performed to verify the absence of negative eigenvalues. Molecular orbital analysis was performed using the bi-orthogonal corresponding orbital approach as implemented in Gaussian 09.

Synthesis of 3. Proligand **1** (1.000 g, 1.889 mmol) was dissolved in THF (1 mL), and 3 equiv of $((CH_3)_3Si)_2NLi$, 97% (0.978 g, 5.669 mmol) in THF (2 mL) were added dropwise to generate the trianionic $[CF_3{-}ONO]^{3-}$ species in situ. This solution was slowly added to a THF (2 mL) solution of $FeCl_3$ (98%, 0.313 g, 1.891 mmol), yielding a blue solution and a significant amount of precipitated LiCl. After stirring the solution for 2 h at room temperature and filtering the inorganic precipitate, the solvent was evaporated under reduced pressure. The resulting blue powder was dissolved in toluene, producing a green solution, which was stirred for 1 h and then filtered to remove the remaining inorganic salts. The solvent was evaporated under reduced pressure. The residue was extracted with THF, and an equal amount of pentane was added. Cooling this solution at −35 °C overnight yielded green crystals (needle shaped) that were isolated and dried under vacuum (1.316 g, 72.9%). ^{1}H NMR (C_6D_6, 300 MHz, 25 °C) δ (ppm): 136.04 ($\nu_{1/2}$ = 360 Hz), 75.55 ($\nu_{1/2}$ = 480 Hz), 16.52 ($\nu_{1/2}$ = 960 Hz), 5.17 ($\nu_{1/2}$ = 360 Hz), and −148.95 ($\nu_{1/2}$ = 240 Hz). Elemental analysis calcd. (%) for $C_{36}H_{44}Cl_2F_{12}FeLi_2NO_6$ (955.35 g/mol): C 45.26, H 4.64, and N 1.47; found: C 45.17, H 4.65, and N 1.42.

Synthesis of 4. Complex **3** (200 mg, 0.209 mmol) was dissolved in DME (1 mL) forming a blue solution. Two equivalents of $TlPF_6$ (97%, 150 mg, 0.416 mmol) were also dissolved in DME (1 mL) and added dropwise to the former solution causing immediate precipitation of TlCl. The resulting green solution was stirred for 20 min and filtered through Celite, and the solvent was removed under reduced pressure. After washing the green residue with pentane (5 mL), the resulting green powder was dissolved in 3 mL of a 2:1 pentane/DME mixture and filtered to remove the remaining inorganic salts. The solvent was removed under reduced pressure. Finally, the green powder was washed with pentane (5 mL) and dried under vacuum. Yield (0.056 g, 37.3%). ^{1}H NMR (C_6D_6, 300 MHz, 25 °C): δ (ppm) = 148.54 ($\nu_{1/2}$ = 360 Hz), 88.38 ($\nu_{1/2}$ = 360 Hz), 77.11 ($\nu_{1/2}$ = 2880 Hz), and −107.93 ($\nu_{1/2}$ = 600 Hz). Elemental analysis calcd (%) for $C_{52}H_{54}F_{24}Fe_2N_2O_{10}$ (1434.64 g/mol): C 43.53, H 3.79, and N 1.95; found: C 43.49, H 3.77, and N 2.00.

Synthesis of 5. Method (a). Complex **4** (80 mg, 0.056 mmol) was dissolved in DME (1 mL), and a DME (1 mL) solution of recrystallized 2,2′-bipyridine (18 mg, 0.115 mmol) was added dropwise producing a bluish-green solution. After the solution was stirred for 20 min, the solvent was removed under reduced pressure, and the solid was washed with pentane (5 mL). Another portion of pentane (2 mL) and DME (1 mL) was added, the resulting suspension was filtered through Celite, and then the filtrate was concentrated under reduced pressure. Cooling a saturated DME/pentane solution to −35 °C yielded green crystals. Yield (0.041 g, 49.8%). ^{1}H NMR (C_6D_6, 300 MHz, 25 °C): δ = 118.72 ($\nu_{1/2}$ = 240 Hz), 92.28 ($\nu_{1/2}$ = 600 Hz), 74.09 ($\nu_{1/2}$ = 360 Hz), 68.13 (480 Hz), −10.79 ($\nu_{1/2}$ = 240 Hz), and −158.39 ($\nu_{1/2}$ = 960 Hz). Elemental analysis calcd (%) for $C_{30}H_{20}F_{12}FeN_3O_2$ (738.07 g/mol): C 48.80, H 2.73, and N 5.69; found: C 48.72, H 2.81, and N 5.76.

Method (b). Complex **3** (200 mg, 0.209 mmol) was dissolved in DME (1 mL) forming a blue solution. $TlPF_6$ (97%, 150 mg, 0.208 mmol) was also dissolved in DME (1 mL) and added dropwise to the former solution causing the immediate precipitation of TlCl. The resulting green solution was stirred for 20 min and then filtered through Celite. A solution of recrystallized 2,2′-bipyridine (0.033 g, 0.211 mmol) in DME (1 mL) was added dropwise producing a bluish-green solution. After the solution was stirred for 20 min, the solvent was removed under reduced pressure, and the solid was washed with pentane (5 mL). Another portion of pentane (2 mL) and DME (1 mL) was added, the resulting suspension was filtered through Celite, and then the filtrate was concentrated under reduced pressure. Cooling a saturated DME/pentane solution to −35 °C yielded green crystals. Yield (0.111 g, 71.8%).

Synthesis of 5·H_2O. The preparation of **5·H_2O** follows the same method as complex **5**; however, wet 2,2′-bipyridine that was not previously recrystallized is used. Yield: 65.7%. ^{1}H NMR (C_6D_6, 300 MHz, 25 °C): δ = 120.14 ($\nu_{1/2}$ = 840 Hz), 94.72 ($\nu_{1/2}$ = 840 Hz), 74.62 ($\nu_{1/2}$ = 600 Hz), 69.85 (720 Hz), −11.11 ($\nu_{1/2}$ = 360 Hz), −93.18 ($\nu_{1/2}$ = 1200 Hz).

■ ASSOCIATED CONTENT

Ⓢ Supporting Information

General experimental considerations, synthesis, X-ray diffraction data, cyclic voltammetry data, additional SQUID data of **3**, and DFT calculation details of **3** and **5**. This material is available free of charge via the Internet at http://pubs.acs.org.

■ AUTHOR INFORMATION

Corresponding Author

*E-mail: veige@chem.ufl.edu.

Notes

The authors declare no competing financial interest.

■ ACKNOWLEDGMENTS

This work was supported, in part, by the National Science Foundation (NSF) via CHE-1265993 (ASV), DMR-1213030 (GC), DMR-1202033 (MWM), DMR-1157490 (NHMFL), and CHE-0821346 (KAA). Research supported by the U.S. Department of Energy, Office of Basic Energy Sciences, Division of Materials Sciences and Engineering under Award DE-FG02-02ER45999 (KRD). ASV also acknowledges UF support and the resources provided by the UF High-Performance Computing Center. NVD is an HHMI International Student Research fellow. We thank Prof. A. Angerhofer and U. Twahir for assistance in the EPR measurements, Prof. A. Roitberg for assistance with DFT calculations, and Dr. E. Čižmár for training on the use of EasySpin codes.

■ REFERENCES

(1) Morales-Morales, D.; Jensen, C. M. *The chemistry of pincer compounds,* 1st ed.; Elsevier: Amsterdam, 2007.

(2) Selander, N.; Szabo, K. J. *Chem. Rev.* **2011**, *111*, 2048−2076.

(3) Leis, W.; Mayer, H. A.; Kaska, W. C. *Coord. Chem. Rev.* **2008**, *252*, 1787−1797.

(4) Benito-Garagorri, D.; Kirchner, K. *Acc. Chem. Res.* **2008**, *41*, 201−213.

(5) O'Reilly, M. E.; Veige, A. S. *Chem. Soc. Rev.* **2014**, *43*, 6325−6369.
(6) Koller, J.; Sarkar, S.; Abboud, K. A.; Veige, A. S. *Organometallics* **2007**, *26*, 5438−5441.
(7) Sarkar, S.; McGowan, K. P.; Culver, J. A.; Carlson, A. R.; Koller, J.; Peloquin, A. J.; Veige, M. K.; Abboud, K. A.; Veige, A. S. *Inorg. Chem.* **2010**, *49*, 5143−5156.
(8) McGowan, K. P.; Abboud, K. A.; Veige, A. S. *Organometallics* **2011**, *30*, 4949−4957.
(9) McGowan, K. P.; Veige, A. S. *J. Organomet. Chem.* **2012**, *711*, 10−14.
(10) Sarkar, S.; McGowan, K. P.; Kuppuswamy, S.; Ghiviriga, I.; Abboud, K. A.; Veige, A. S. *J. Am. Chem. Soc.* **2012**, *134*, 4509−4512.
(11) Sarkar, S.; Carlson, A. R.; Veige, M. K.; Falkowski, J. M.; Abboud, K. A.; Veige, A. S. *J. Am. Chem. Soc.* **2008**, *130*, 1116−1117.
(12) Sarkar, S.; Abboud, K. A.; Veige, A. S. *J. Am. Chem. Soc.* **2008**, *130*, 16128−16129.
(13) O'Reilly, M. E.; Del Castillo, T. J.; Falkowski, J. M.; Ramachandran, V.; Pati, M.; Correia, M. C.; Abboud, K. A.; Dalal, N. S.; Richardson, D. E.; Veige, A. S. *J. Am. Chem. Soc.* **2011**, *133*, 13661−13673.
(14) O'Reilly, M.; Falkowski, J. M.; Ramachandran, V.; Pati, M.; Abboud, K. A.; Dalal, N. S.; Gray, T. G.; Veige, A. S. *Inorg. Chem.* **2009**, *48*, 10901−10903.
(15) O'Reilly, M. E.; Castillo, T. J. D.; Abboud, K. A.; Veige, A. S. *Dalton Trans.* **2012**, *41*, 2237−2246.
(16) Kuppuswamy, S.; Peloquin, A. J.; Ghiviriga, I.; Abboud, K. A.; Veige, A. S. *Organometallics* **2010**, *29*, 4227−4233.
(17) Kuppuswamy, S.; Ghiviriga, I.; Abboud, K. A.; Veige, A. S. *Organometallics* **2010**, *29*, 6711−6722.
(18) McGowan, K. P.; O'Reilly, M. E.; Ghiviriga, I.; Abboud, K. A.; Veige, A. S. *Chem. Sci.* **2013**, *4*, 1145−1155.
(19) Golisz, S. R.; Labinger, J. A.; Bercaw, J. E. *Organometallics* **2010**, *29*, 5026−5032.
(20) Agapie, T.; Day, M. W.; Bercaw, J. E. *Organometallics* **2008**, *27*, 6123−6142.
(21) Agapie, T.; Bercaw, J. E. *Organometallics* **2007**, *26*, 2957−2959.
(22) Cladis, D. P.; Kiernicki, J. J.; Fanwick, P. E.; Bart, S. C. *Chem. Commun.* **2013**, *49*, 4169−4171.
(23) Schrock, R. R.; Lee, J.; Liang, L.; Davis, W. M. *Inorg. Chim. Acta* **1998**, *270*, 353−362.
(24) Nguyen, A. I.; Blackmore, K. J.; Carter, S. M.; Zarkesh, R. A.; Heyduk, A. F. *J. Am. Chem. Soc.* **2009**, *131*, 3307−3316.
(25) Heyduk, A. F.; Zarkesh, R. A.; Nguyen, A. I. *Inorg. Chem.* **2011**, *50*, 9849−9863.
(26) Tondreau, A. M.; Stieber, S. C.; Milsmann, C.; Lobkovsky, E.; Weyhermüller, T.; Semproni, S. P.; Chirik, P. J. *Inorg. Chem.* **2013**, *52*, 635−646.
(27) Sattler, A.; Parkin, G. *J. Am. Chem. Soc.* **2012**, *134*, 2355−2366.
(28) Shaffer, D. W.; Szigethy, G.; Ziller, J. W.; Heyduk, A. F. *Inorg. Chem.* **2013**, *52*, 2110−2118.
(29) O'Reilly, M. E.; Nadif, S. S.; Ghiviriga, I.; Abboud, K. A.; Veige, A. S. *Organometallics* **2014**, *33*, 836−839.
(30) O'Reilly, M. E.; Ghiviriga, I.; Abboud, K. A.; Veige, A. S. *Dalton Trans.* **2013**, *42*, 3326−3336.
(31) O'Reilly, M. E.; Ghiviriga, I.; Abboud, K. A.; Veige, A. S. *J. Am. Chem. Soc.* **2012**, *134*, 11185−11195.
(32) VenkatRamani, S.; Pascualini, M. E.; Ghiviriga, I.; Abboud, K. A.; Veige, A. S. *Polyhedron* **2013**, *64*, 377−387.
(33) Pascualini, M. E.; Di Russo, N. V.; Thuijs, A. E.; Ozarowski, A.; Stoian, S.; Abboud, K. A.; Christou, G.; Veige, A. S. *Chem. Sci.* **2014**, DOI: 10.1039/c4sc02634a.
(34) Wong, J. L.; Hernandez Sanchez, R.; Glancy Logan, J.; Zarkesh, R. A.; Ziller, J. W.; Heyduk, A. F. *Chem. Sci.* **2013**, *4*, 1906−1910.
(35) Zarkesh, R. A.; Heyduk, A. F. *Organometallics* **2011**, *30*, 4890−4898.
(36) Zarkesh, R. A.; Ziller, J. W.; Heyduk, A. F. *Angew. Chem., Int. Ed.* **2008**, *47*, 4715−4718.
(37) Munhá, R. F.; Zarkesh, R. A.; Heyduk, A. F. *Dalton Trans.* **2013**, *42*, 3751−3766.
(38) Zarkesh, R. A.; Heyduk, A. F. *Organometallics* **2009**, *28*, 6629−6631.
(39) Girgis, A. Y.; Balch, A. L. *Inorg. Chem.* **1975**, *14*, 2724−2727.
(40) Simpson, C. L.; Boone, S. R.; Pierpont, C. G. *Inorg. Chem.* **1989**, *28*, 4379−4385.
(41) Larsen, S. K.; Pierpont, C. G. *J. Am. Chem. Soc.* **1988**, *110*, 1827−1832.
(42) Pierpont, C. G.; Larsen, S. K.; Boone, S. R. *Pure Appl. Chem.* **1988**, *60*, 1331−1336.
(43) Chaudhuri, P.; Hess, M.; Weyhermuller, T.; Wieghardt, K. *Angew. Chem., Int. Ed.* **1999**, *38*, 1095−1098.
(44) Darmon, J. M.; Stieber, S. C. E.; Sylvester, K. T.; Fernandez, I.; Lobkovsky, E.; Semproni, S. P.; Bill, E.; Wieghardt, K.; DeBeer, S.; Chirik, P. J. *J. Am. Chem. Soc.* **2012**, *134*, 17125−17137.
(45) Addison, A. W.; Nageswara Rao, T.; Reedijk, J.; van Rijn, J.; Verschoor, G. C. *J. Chem. Soc., Dalton Trans.* **1984**, 1349−1356.
(46) Mossin, S.; Tran, B. L.; Adhikari, D.; Pink, M.; Heinemann, F. W.; Sutter, J.; Szilagyi, R. K.; Meyer, K.; Mindiola, D. J. *J. Am. Chem. Soc.* **2012**, *134*, 13651−13661.
(47) Figgis, B. N.; Skelton, B. W.; White, A. H. *Aust. J. Chem.* **1978**, *31*, 57−64.
(48) Kadish, K. M.; Larson, G.; Lexa, D.; Momenteau, M. *J. Am. Chem. Soc.* **1975**, *97*, 282−288.
(49) Gueutin, C.; Lexa, D.; Saveant, J.; Wang, D. *Organometallics* **1989**, *8*, 1607−1613.
(50) Collomb, M. N.; Deronzier, A.; Gorgy, K.; Lepretre, J. C.; Pecaut, J. *New J. Chem.* **1999**, *23*, 785−790.
(51) Grodkowski, J.; Neta, P.; Fujita, E.; Mahammed, A.; Simkhovich, L.; Gross, Z. *J. Phys. Chem. A* **2002**, *106*, 4772−4778.
(52) Van Caemelbecke, E.; Will, S.; Autret, M.; Adamian, V. A.; Lex, J.; Gisselbrecht, J.; Gross, M.; Vogel, E.; Kadish, K. M. *Inorg. Chem.* **1996**, *35*, 184−192.
(53) Stoll, S.; Schweiger, A. *J. Magn. Reson.* **2006**, *178*, 42−55.
(54) Krzystek, J.; Ozarowski, A.; Telser, J. *Coord. Chem. Rev.* **2006**, *250*, 2308−2324.
(55) Sazama, G. T.; Betley, T. A. *Inorg. Chem.* **2014**, *53*, 269−281.
(56) Solomon, E.; Brunold, T.; Davis, M.; Kemsley, J.; Lee, S.; Lehnert, N.; Neese, F.; Skulan, A.; Yang, Y.; Zhou, J. *Chem. Rev.* **2000**, *100*, 235−349.
(57) Evans, D. F. *J. Chem. Soc.* **1959**, 2003−2005.
(58) Guillet, G. L.; Sloane, F. T.; Ermert, D. M.; Calkins, M. W.; Peprah, M. K.; Knowles, E. S.; Čižmár, E.; Abboud, K. A.; Meisel, M. W.; Murray, L. J. *Chem. Commun.* **2013**, *49*, 6635−6637.
(59) Becke, A. D. *J. Chem. Phys.* **1993**, *98*, 5648−5652.
(60) Lee, C.; Yang, W.; Parr, R. G. *Phys. Rev. B* **1988**, *37*, 785−789.
(61) Allard, M. M.; Sonk, J. A.; Heeg, M. J.; McGarvey, B. R.; Schlegel, H. B.; Verani, C. N. *Angew. Chem., Int. Ed.* **2012**, *51*, 3178−3182.
(62) Chiang, L.; Savard, D.; Shimazaki, Y.; Thomas, F.; Storr, T. *Inorg. Chem.* **2014**, *53*, 5810−5819.
(63) Sherry, B. D.; Fürstner, A. *Acc. Chem. Res.* **2008**, *41*, 1500−1511.
(64) Enthaler, S.; Junge, K.; Beller, M. *Angew. Chem., Int. Ed.* **2008**, *47*, 3317−3321.
(65) Frisch, M. J.; Trucks, G. W.; Schlegel, H. B.; Scuseria, G. E.; Robb, M. A.; Cheeseman, J. R.; Scalmani, G.; Barone, V.; Mennucci, B.; Petersson, G. A.; Nakatsuji, H.; Caricato, M.; Li, X.; Hratchian, H. P.; Izmaylov, A. F.; Bloino, J.; Zheng, G.; Sonnenberg, J. L.; Hada, M.; Ehara, M.; Toyota, K.; Fukuda, R.; Hasegawa, J.; Ishida, M.; Nakajima, T.; Honda, Y.; Kitao, O.; Nakai, H.; Vreven, T.; Montgomery, J. J. A.; Peralta, J. E.; Ogliaro, F.; Bearpark, M.; Heyd, J. J.; Brothers, E.; Kudin, K. N.; Staroverov, V. N.; Keith, T.; Kobayashi, R.; Normand, J.; Raghavachari, K.; Rendell, A.; Burant, J. C.; Iyengar, S. S.; Tomasi, J.; Cossi, M.; Rega, N.; Millam, J. M.; Klene, M.; Knox, J. E.; Cross, J. B.; Bakken, V.; Adamo, C.; Jaramillo, J.; Gomperts, R.; Stratmann, R. E.; Yazyev, O.; Austin, A. J.; Cammi, R.; Pomelli, C.; Ochterski, J. W.; Martin, R. L.; Morokuma, K.; Zakrzewski, V. G.; Voth, G. A.; Salvador, P.; Dannenberg, J. J.; Dapprich, S.; Daniels, A. D.; Farkas, O.;

Foresman, J. B.; Ortiz, J. V.; Cioslowski, J.; Fox, D. J. *Gaussian 09*, Revision D.01; Gaussian, Inc.: Wallingford, CT, 2013.
(66) Hay, P. J.; Wadt, W. R. *J. Chem. Phys.* **1985**, *82*, 270−283.